



## Fast and dephasing-tolerant preparation of steady Knill-Laflamme-Milburn states via dissipative Rydberg pumping

Ri-Hua Zheng <sup>1,2</sup> Yang Xiao,<sup>1,2</sup> S.-L. Su,<sup>3,\*</sup> Ye-Hong Chen <sup>4</sup> Zhi-Cheng Shi,<sup>1,2</sup> Jie Song,<sup>5</sup>  
Yan Xia,<sup>1,2,†</sup> and Shi-Biao Zheng<sup>1,2</sup>

<sup>1</sup>Fujian Key Laboratory of Quantum Information and Quantum Optics (Fuzhou University), Fuzhou 350108, China

<sup>2</sup>Department of Physics, Fuzhou University, Fuzhou 350108, China

<sup>3</sup>School of Physics, Zhengzhou University, Zhengzhou 450001, China

<sup>4</sup>Theoretical Quantum Physics Laboratory, RIKEN Cluster for Pioneering Research, Wako-shi, Saitama 351-0198, Japan

<sup>5</sup>Department of Physics, Harbin Institute of Technology, Harbin 150001, China



(Received 6 October 2020; revised 21 February 2021; accepted 19 April 2021; published 4 May 2021)

We propose a fast and dephasing-tolerant scheme for the preparation of steady Knill-Laflamme-Milburn (KLM) state between a pair of Rydberg atoms by dissipation. In this scheme, arbitrary initial state can be engineered to the KLM state with high fidelity (99.24%). Compared to most schemes based on Rydberg dissipation dynamics, the time to prepare steady state can be significantly reduced in our scheme (80  $\mu$ s) due to the use of strong resonant dipole-dipole interactions. In addition, the scheme can effectively suppress the dephasing error of the Rydberg atoms caused by interatomic distance fluctuations, which may severely disrupt the desired systematic dynamics. Thus the present scheme is of interest and deserves further experimental investigation to enrich the dissipation dynamics based on the Rydberg atoms.

DOI: [10.1103/PhysRevA.103.052402](https://doi.org/10.1103/PhysRevA.103.052402)

### I. INTRODUCTION

Entanglement plays a central role in quantum mechanics and has been actively applied to various types of quantum information processing (QIP) tasks, such as quantum teleportation [1–3], quantum cryptography [4–6], and quantum state sharing [7,8]. Among various methods for producing entanglement, the dissipative preparation [9–21] is a preponderant one, since it transforms the stumbling block of unitary-dynamics preparation, dissipation, into engineering resource. That is, by using the dissipative preparation, the fidelity is generally insensitive to the dissipation and therefore gives rise to higher fidelity, which has been experimentally demonstrated in macroscopic systems [22], ionic systems [23,24], and superconducting systems [25].

Recently, due to the superior properties of strong dipole-dipole interactions and long lifetimes of Rydberg atoms [26], some interest has been attracted in Rydberg-atom-based dissipative preparation [16,17,19,27–37]. For instance, Carr *et al.* [16] extended the Rydberg-atom-based dissipative preparation to produce Bell states within 50 ms with fidelity 99.8%. Subsequent works studied multi-dimensional-entanglement preparation scheme [30] and simplified scheme [31] for the Rydberg-atom-based dissipative preparation with evolution times about 300 and 200 ms, respectively. Generally, the evolution times with tens to hundreds of milliseconds of above schemes seem too long for some fast QIP tasks and should be further shorten. Thereby, an alternative scheme, by

utilizing the electromagnetically induced transparency (EIT) phenomenon [38], was proposed by Rao *et al.* [17] with a shorter evolution time 50  $\mu$ s. While the scheme may face some possible difficulties that the simultaneous excitations of multiple Rydberg states will induce the dephasing noise in the experiment.

Indeed, the dephasing of Rydberg atoms always be seen as an obstacle lying on the application of Rydberg-atom-based QIP. Generally, the atoms in optical tweezers will slightly vibrate and therefore leads to the atomic dephasing [39]. Such a phenomenon will bring small change of the dipole-dipole interaction energy (scaling by  $1/R^3$  or  $1/R^6$ ) and may seriously destroy the desired systematic dynamics when more than one Rydberg states are excited during the evolution. For instance, in the experiment [39], the damping of the desired oscillations reached about 50% within only 700 ns (see Fig. 3(b) in Ref. [39]) due to the atomic dephasing induced by simultaneously exciting Rydberg atoms.

Here we propose a dissipative scheme to try to address the issues of long time required and sensitivity to dephasing noise. Specifically, the bipartite Knill-Laflamme-Milburn (KLM) state [40], which can be used to significantly improve the success probability of QIP tasks, is taken here as an example to illustrate our dynamics. We use the strong resonant dipole-dipole interaction [36,37,39] (scaling as  $1/R^3$  [41,42]) instead of the relatively weak van der Waals interaction (scaling as  $1/R^6$  [43]). The big interaction energy allows us to apply relatively strong driving fields and choose dissipative states with higher dissipation rates, yielding a shorter evolution time (80  $\mu$ s with fidelity 99.24%). Additionally, we avoid multiple Rydberg states excitations for the Rydberg atoms, which reduces the complexity of the experiment and also attenuates

\*slsu@zzu.edu.cn

†xia-208@163.com

the effects of dephasing noise [39]. The numerical simulation shows that when we consider the interaction energy fluctuation rate as 6% [39], the fidelity in the present scheme is still high as 97.36% at 80  $\mu$ s (the infidelity will accumulate over time), which strongly proves that the present scheme is effective in suppressing the atomic dephasing. Moreover, our scheme can also (i) deal with another potential source of experimental error induced by voltage fluctuation, (ii) be robust to the Rabi frequencies deviations, and (iii) possesses fine arbitrariness of the initial state (either any form of pure states or any form of mixed states can be used to prepare the target state).

The paper is organized as follows. In Sec. II, we introduce the physical model for the fast and dephasing-tolerant preparation of steady KLM states in detail, whose dynamic is studied in Sec. III. In Sec. IV, we give the numerical simulation of the present scheme by considering atomic dephasing, voltage fluctuation, Rabi frequencies deviations, and arbitrariness of the initial state. Finally the discussion is given in Sec. V.

## II. PHYSICAL MODEL FOR THE FAST AND DEPHASING-TOLERANT PREPARATION OF STEADY KLM STATES

The KLM state produced here is bipartite, given by [40]

$$|\text{KLM}\rangle = \frac{1}{\sqrt{3}}(|00\rangle + |10\rangle + |11\rangle). \quad (1)$$

The physical model for preparing the KLM states is shown in Fig. 1(a), a pair of  $^{87}\text{Rb}$  atoms trapped at a distance of  $R = 2.673 \mu\text{m}$  in two optical tweezers, whose interatomic axis is aligned with a magnetic field ( $B = 9 \text{ G}$ ). Here we use the states  $|p\rangle = |61P_{1/2}, m_j = 1/2\rangle$ ,  $|r\rangle = |59D_{3/2}, m_j = 3/2\rangle$ ,  $|f\rangle = |57F_{5/2}, m_j = 5/2\rangle$ ,  $|e\rangle = |9P_{3/2}, F = 2, m_F = 0\rangle$ ,  $|0\rangle = |5S_{1/2}, F = 1, m_F = 0\rangle$ , and  $|1\rangle = |5S_{1/2}, F = 2, m_F = 0\rangle$  of  $^{87}\text{Rb}$ . The pair states  $|rr\rangle$  and  $|pf\rangle$  [ $|pf\rangle = (|pf\rangle + |fp\rangle)/\sqrt{2}$ ] are almost degenerate [41,42], with a relatively small energy difference named ‘Förster defect’, which can be quantified as  $\Delta_0 = (E_{pf} - E_{rr})/h = 8.5 \text{ MHz}$  ( $h$  being the Planck’s constant). For eliminating the Förster defect, an electric field  $F_{\text{res}} \simeq 32 \text{ mVcm}^{-1}$  [39] is added to the  $^{87}\text{Rb}$  atoms, which compensates the Förster defect because of different Stark effect between  $|rr\rangle$  and  $|pf\rangle$ . By now, a strict ‘Förster resonance’ is constructed well and in this case the dipole-dipole interaction is strong with  $V_{\text{dip}} = \sqrt{2}C_3/R^3$ , where  $C_3/h = 2.54 \text{ GHz } \mu\text{m}^3$  was ideally given by the theory of [44] and  $C_3/h = 2.39 \pm 0.03 \text{ GHz } \mu\text{m}^3$  was measured in the experiment [39].

Figure 1(b) shows the level diagrams of atoms for the present scheme, in which ground state  $|1\rangle_1$  and Rydberg state  $|r(p)\rangle_1$  is coupled by a laser field with Rabi frequency  $\Omega_1$  and blue (red) detuning  $\Delta$  in atom 1. As for atom 2,  $|r\rangle_2$  and  $|1(e)\rangle_2$  are resonantly coupled by a laser field with Rabi frequency  $\Omega_2$  ( $\Omega_e$ ). Note that  $|1\rangle \leftrightarrow |r(p)\rangle$  is indeed a two-photon transition constructed by a  $\sigma^+$ -polarized 480 nm laser and a  $\sigma^-$ -polarized 784 nm laser [see Fig. 1(c)], which has been experimentally realized [45]. Additionally, the transitions of  $|0\rangle_1 \leftrightarrow |1\rangle_1$  and  $|0\rangle_2 \leftrightarrow |1\rangle_2$  are driven by two Raman

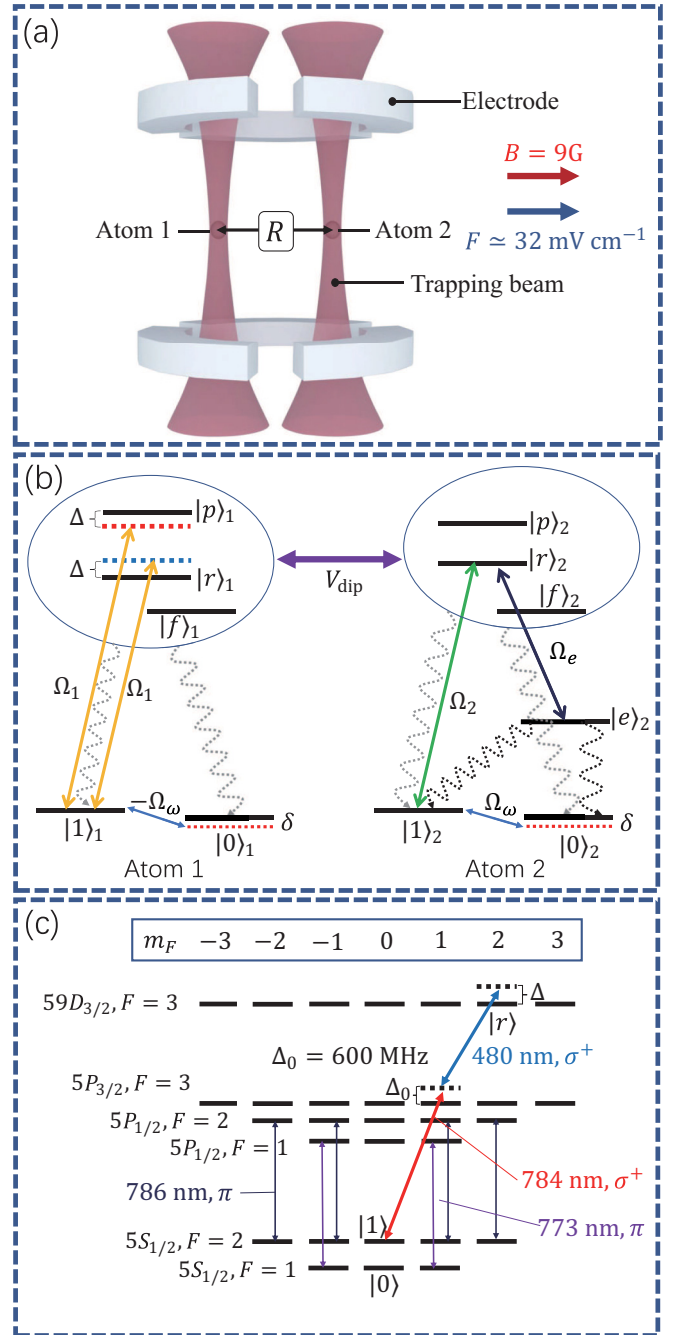


FIG. 1. (a) Imagined experimental model diagram. (b) Level diagrams of atoms. The gray and black curved arrows represent dissipation ways from Rydberg states ( $|p\rangle$ ,  $|r\rangle$ , and  $|f\rangle$ ) and intermediate excited state  $|e\rangle$  to ground states, respectively. (c) Detailed schematic about how the two-photon transition and recycling lasers work. Only two-photon transition  $|1\rangle \leftrightarrow |r\rangle$  is plotted because  $|1\rangle \leftrightarrow |p\rangle$  is easy to be analogized. In addition, the dark blue and purple arrows, respectively representing two  $\pi$ -polarized lasers at about 786 nm and 773 nm, can recycle all the other Zeeman ground states to  $|0\rangle$  and  $|1\rangle$ .

laser fields [46] with Rabi frequencies  $-\Omega_\omega$  and  $\Omega_\omega$ , respectively, whose detunings are all  $\delta$ .

Also, the Rydberg states ( $|p\rangle$ ,  $|r\rangle$ , and  $|f\rangle$ ) and intermediate excited state ( $|e\rangle$ ) can decay to ground states with spontaneous

emission rates  $\Gamma_{(p,r,f)}$  and  $\Gamma_e$ , respectively. It is worth mentioning that the ground states are not just  $|0\rangle$  and  $|1\rangle$  plotted in Fig. 1(b). Generally, for  $^{87}\text{Rb}$  atoms, there are eight ground states  $|5S_{1/2}, F=1, m_F=0, \pm 1\rangle$  and  $|5S_{1/2}, F=2, m_F=0, \pm 1, \pm 2\rangle$ , and the decay rate of the spontaneous emission to one of these eight states is proportional to the corresponding dipole moment between that ground state and  $|5P_{3/2}, F=3\rangle$  state. Nevertheless, here we add two  $\pi$ -polarized lasers at about 786 nm and 773 nm [see Fig. 1(c)] to pump all the ground states except  $|0\rangle$  and  $|1\rangle$  up to  $|5P_{1/2}\rangle$  because transition  $|m_F=0\rangle \rightarrow |m_F=0\rangle$  is forbidden according to the selection rule. Furthermore, the spontaneous emission rate state  $|5P_{1/2}\rangle$  is huge as 36.98 MHz [47], inducing rapidly decaying from  $|5P_{1/2}\rangle$  to ground states and the ground states will be pumped up again. Therefore, in this setting, it is reasonable to assume that  $|0\rangle$  and  $|1\rangle$  can be the end states of the spontaneous emission, and we consider them as representatives of the ground states [16].

### III. DYNAMIC OF THE PHYSICAL MODEL

The total Hamiltonian of the physical model in the interaction picture yields ( $\hbar = 1$  hereafter)

$$\begin{aligned} H &= \Omega_1 e^{i\Delta t} |p\rangle_1 \langle 1| + \Omega_1 e^{-i\Delta t} |r\rangle_1 \langle 1| + \Omega_2 |r\rangle_2 \langle 1| \\ &\quad + \Omega_e |r\rangle_2 \langle e| + V_{\text{dip}} |rr\rangle \langle \widetilde{p}f| + \text{H.c.} + H_\omega, \\ H_\omega &= \Omega_\omega (-|0\rangle_1 \langle 1| + |0\rangle_2 \langle 1|) + \text{H.c.} \\ &\quad + \delta(|0\rangle_1 \langle 0| + |0\rangle_2 \langle 0|). \end{aligned} \quad (2)$$

The term of Förster resonance,  $V_{\text{dip}} |rr\rangle \langle \widetilde{p}f| + \text{H.c.}$ , can be diagonalized as  $V_{\text{dip}}(|+\rangle\langle +| - |-\rangle\langle -|)$  with  $|\pm\rangle = (|rr\rangle \pm |\widetilde{p}f\rangle)/\sqrt{2}$ . Here we set  $\Delta = V_{\text{dip}} \gg \Omega_1$  and move into a new picture with a rotating frame  $R = \exp[iV_{\text{dip}}t(|+\rangle\langle +| - |-\rangle\langle -|)]$ , giving rise to (assuming the initial state elements all made up by ground states)

$$H' = RHR^\dagger + i\dot{R}R^\dagger = H_1 + H_2 + H_\omega, \quad (3)$$

where  $H_1$  and  $H_2$  are resonant and high-frequency part of  $H - H_\omega$ , respectively, given by

$$\begin{aligned} H_1 &= \Omega_2(|01\rangle\langle 0r| + |11\rangle\langle 1r| + |p1\rangle\langle pr|) + \frac{\Omega_1}{\sqrt{2}}|1r\rangle\langle +| \\ &\quad + \Omega_e(|0r\rangle\langle 0e| + |1r\rangle\langle 1e| + |pr\rangle\langle pe|) + \text{H.c.}, \\ H_2 &= \Omega_1 e^{i\Delta t}(|10\rangle\langle r0| + |p0\rangle\langle 10| + |11\rangle\langle r1| \\ &\quad + |p1\rangle\langle 11| + |1e\rangle\langle re| + |pe\rangle\langle 1e| + |pr\rangle\langle r1|) \\ &\quad + \frac{1}{\sqrt{2}}e^{-i\Delta t}|-\rangle(\Omega_2\langle r1| + \Omega_e\langle re|) \\ &\quad + \frac{1}{\sqrt{2}}e^{-i\Delta t}(\Omega_2|r1\rangle + \Omega_e|re\rangle)\langle +| \\ &\quad + \frac{\Omega_1}{\sqrt{2}}e^{2i\Delta t}|1r\rangle\langle -| + \text{H.c.} \end{aligned} \quad (4)$$

Note that some terms containing states  $|e\rangle_1, |f\rangle_1, |f\rangle_2$ , and  $|p\rangle_2$  have been neglected since they are decoupled to the system. An intuitive explanation is that there is no corresponding lasers drive other states to  $|e\rangle_1, |f\rangle_1, |f\rangle_2$ , and  $|p\rangle_2$  [see Fig. 1(b)]. Further more, we can calculate the effective value

of  $H_2$  by time-averaged dynamic [48], a precise method of second-order perturbation theory, yielding

$$\begin{aligned} H_{2\text{eff}} &= \sum_{u=1}^2 [h_u^\dagger, h_u]/\omega_u \\ &= \frac{\Omega_1^2}{\Delta}(|p0\rangle\langle p0| - |r0\rangle\langle r0| + |p1\rangle\langle p1| - |r1\rangle\langle r1| \\ &\quad + |pr\rangle\langle pr| - |1r\rangle\langle 1r| + |pe\rangle\langle pe| - |re\rangle\langle re|) \\ &\quad + \frac{\Omega_2^2 + \Omega_e^2}{2\Delta}(|+\rangle\langle +| - |-\rangle\langle -|) \\ &\quad + \frac{\Omega_1\Omega_e}{\sqrt{2}\Delta}(|+\rangle\langle 1e| + |1e\rangle\langle +|) \\ &\quad + \frac{\Omega_1^2}{4\Delta}(|1r\rangle\langle 1r| - |-\rangle\langle -|), \end{aligned} \quad (5)$$

with

$$\begin{aligned} h_1^\dagger &= \Omega_1(|10\rangle\langle r0| + |p0\rangle\langle 10| + |11\rangle\langle r1| \\ &\quad + |p1\rangle\langle 11| + |1e\rangle\langle re| + |pe\rangle\langle 1e| + |pr\rangle\langle r1|) \\ &\quad + \frac{1}{\sqrt{2}}|+\rangle(\Omega_2\langle r1| + \Omega_e\langle re|) \\ &\quad + \frac{1}{\sqrt{2}}(\Omega_2|r1\rangle + \Omega_e|re\rangle)\langle -|, \\ h_2^\dagger &= \frac{\Omega_1}{\sqrt{2}}|1r\rangle\langle -|, \end{aligned} \quad (6)$$

corresponding to high frequencies  $\Delta$  and  $2\Delta$ , respectively. Therefore, by additionally neglecting some decoupled terms and assuming  $\Omega_1 \gg \{\Omega_2, \Omega_e, \Omega_\omega\}$ , the total Hamiltonian can be refined as

$$\begin{aligned} H' &\simeq H_1 + H_{2\text{eff}} + H'_\omega \\ &\simeq \Omega_2(|01\rangle\langle 0r| + |11\rangle\langle 1r|) \\ &\quad + \Omega_e(|0r\rangle\langle 0e| + |1e\rangle\langle 1r|) - \Omega_\omega(|0r\rangle\langle 1r| + |0e\rangle\langle 1e|) \\ &\quad + \frac{\Omega_1}{\sqrt{2}}|1r\rangle\langle +| + \text{H.c.} - \frac{3\Omega_1^2}{4\Delta}|1r\rangle\langle 1r| \\ &\quad + \delta(|0r\rangle\langle 0r| + |0e\rangle\langle 0e|) + H'_\omega, \end{aligned} \quad (7)$$

where  $H'_\omega$  contains no excited state ( $|e\rangle, |r\rangle, |p\rangle$ , and  $|f\rangle$ ), reading

$$\begin{aligned} H'_\omega &= \Omega_\omega(-|00\rangle\langle 10| - |01\rangle\langle 11| \\ &\quad + |00\rangle\langle 01| + |10\rangle\langle 11|) + \text{H.c.} \\ &\quad + \delta(2|00\rangle\langle 00| + |01\rangle\langle 01| + |10\rangle\langle 10|). \end{aligned} \quad (8)$$

Here, the condition,  $\Omega_1 \gg \{\Omega_2, \Omega_e, \Omega_\omega\}$  is applied to obtain the effective Hamiltonian. We diagonalize the relatively huge part of Eq. (7),  $\frac{\Omega_1}{\sqrt{2}}|1r\rangle\langle +| + \text{H.c.}$ , as  $\frac{\Omega_1}{\sqrt{2}}(|E_+\rangle\langle E_+| - |E_-\rangle\langle E_-|)$  with  $|E_\pm\rangle = (|1r\rangle \pm |+\rangle)/\sqrt{2}$ . In such a situation,

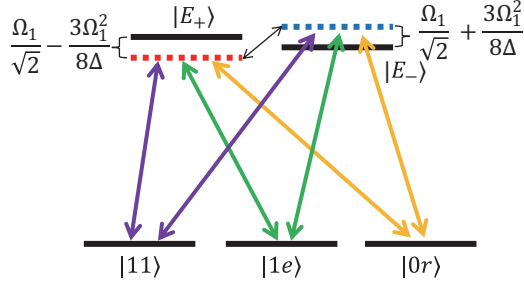


FIG. 2. Schematic of the effective model described Eq. (9), in the absence of resonant part. Observe that the purple, green, yellow, and black arrows represent laser pulses with Rabi frequencies  $\frac{\Omega_2}{\sqrt{2}}$ ,  $\frac{\Omega_e}{\sqrt{2}}$ ,  $-\frac{\Omega_\omega}{\sqrt{2}}$ , and  $\frac{3\Omega_1^2}{8\Delta}$ , respectively.

$H'$  becomes

$$\begin{aligned}
 H' \simeq & \Omega_2 \left[ |01\rangle\langle 0r| + \frac{1}{\sqrt{2}} |11\rangle(\langle E_+| + \langle E_-|) \right] \\
 & + \Omega_e \left[ |0r\rangle\langle 0e| + \frac{1}{\sqrt{2}} |1e\rangle(\langle E_+| + \langle E_-|) \right] \\
 & - \Omega_\omega \left[ \frac{1}{\sqrt{2}} |0r\rangle(\langle E_+| + \langle E_-|) + |0e\rangle\langle 1e| \right] \\
 & + \text{H.c.} + \delta(|0r\rangle\langle 0r| + |0e\rangle\langle 0e|) \\
 & - \frac{3\Omega_1^2}{8\Delta} (|E_+\rangle + |E_-\rangle)(\langle E_+| + \langle E_-|) \\
 & + \frac{\Omega_1}{\sqrt{2}} (|E_+\rangle\langle E_+| - |E_-\rangle\langle E_-|) + H'_\omega. \quad (9)
 \end{aligned}$$

From Eq. (9) and Fig. 2, it is clear that state  $\frac{1}{\sqrt{2}}(|E_+\rangle + |E_-\rangle)$ , i.e.,  $|1r\rangle$ , is decoupled to states  $|11\rangle$ ,  $|1e\rangle$ , and  $|0r\rangle$ , with huge detuning like  $(\frac{\Omega_1}{\sqrt{2}} - \frac{3\Omega_1^2}{8\Delta})|E_+\rangle\langle E_+| - (\frac{\Omega_1}{\sqrt{2}} + \frac{3\Omega_1^2}{8\Delta})|E_-\rangle\langle E_-|$ . Hence the final effective Hamiltonian yields

$$\begin{aligned}
 H_{\text{eff}} &= H_p + H'_\omega, \\
 H_p &= \Omega_2 |01\rangle\langle 0r| + \Omega_e |0r\rangle\langle 0e| - \Omega_\omega |0e\rangle\langle 1e| + \text{H.c.} \\
 &+ \delta(|0r\rangle\langle 0r| + |0e\rangle\langle 0e|), \quad (10)
 \end{aligned}$$

where  $H_p$  is the pumping Hamiltonian that continuously drives the ground state  $|01\rangle$  to excited states  $|0r\rangle$ ,  $|0e\rangle$ , and  $|1e\rangle$ , and  $H'_\omega$  [see Eq. (8)] is the ‘shuffling Hamiltonian’, constantly disrupting the distribution of the ground states.

We firstly focus on the pumping Hamiltonian  $H_p$ . For comparison, we plot schematic diagrams of  $H_p$  driven system, Rydberg anti-blockade system [49–54], and Rydberg blockade system in Figs. 3(a), 3(b), and 3(c), respectively. From Fig. 3(a), it is clear that, among four ground states, only  $|01\rangle$  can be pumped up to single-Rydberg state  $|0r\rangle$  (coupled to  $|0e\rangle$  and  $|1e\rangle$ ), and then decays to the ground states. These excitation and dissipative processes will repeat many times until the target state is achieved. The Rydberg anti-blockade effect shown in Fig. 3(b) induces a similar process as  $H_p$  driven system, however, with a drawback that double-Rydberg states  $|rr\rangle$  is involved in the evolution. In the current experimental scheme [39], due to the finite temperature of the atoms in the tweezers, there is a inevitable

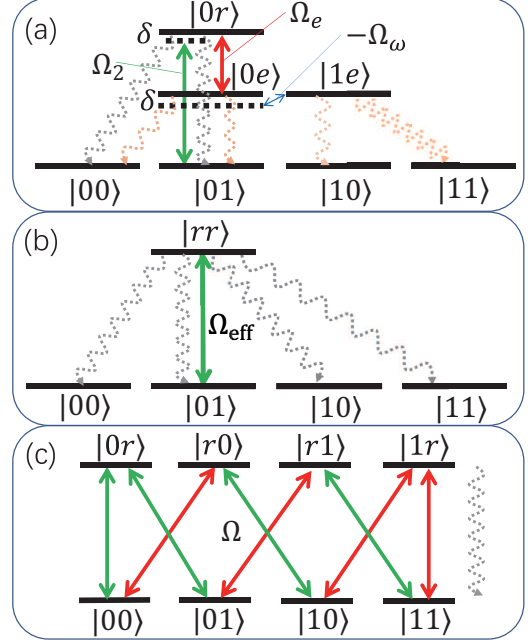


FIG. 3. Illustrations of (a)  $H_p$  driven system, (b) Rydberg anti-blockade system, and (c) Rydberg blockade system. The curved arrows represent dissipation ways caused by spontaneous emission of the excited states.

fluctuation distance between  $^{87}\text{Rb}$  atoms, specifically,  $\delta R = 170$  nm when  $R \simeq 9$   $\mu\text{m}$  ( $\delta V_{\text{dip}}/V_{\text{dip}} \simeq 3\delta R/R \sim 6\%$ ). Such a phenomenon will destroy the accuracy of the effective Hamiltonian (like  $H_{\text{eff}} = \Omega_{\text{eff}}|01\rangle\langle rr| + \text{H.c.}$ ) of the Rydberg anti-blockade system since  $\Omega_{\text{eff}}$  and  $\delta V_{\text{dip}}$  may be of the same order of magnitude (detailed discussion shown in Sec. IV B). In contrast,  $H_p$  driven system in the present scheme can avoid this problem because only single-Rydberg state is pumped.

Additionally, for the Rydberg blockade effect shown in Fig. 3(c), one can find that, only single-Rydberg states ( $|0r\rangle$ ,  $|r0\rangle$ ,  $|r1\rangle$ , and  $|1r\rangle$ ) are stimulated, which indicates that the Rydberg blockade system is not sensitive to the fluctuations of atomic distance, as well. Nevertheless, the Rydberg blockade effect generally pumps ground states without strict selectivity. For instance, in Fig. 3(c), all ground states can be stimulated to the single-Rydberg states, hence leading to instability of all the ground states. On the contrary, system driven by  $H_p$  in the present scheme can construct the stability of  $|00\rangle$ ,  $|10\rangle$ , and  $|11\rangle$  and is useful for the preparation of steady KLM states.

To illustrate the stability, the populations of ground states driven by (without dissipation) the effective pumping Hamiltonian  $H_p$  and original pumping Hamiltonian  $H - H'_\omega$  shown in Eqs. (2, 8) versus time are plotted in Fig. 4. As shown in Fig. 4, the populations of  $|00\rangle$ ,  $|10\rangle$ , and  $|11\rangle$  driven by the Hamiltonian  $H_p$ , are almost invariable. While the population of  $|01\rangle$  driven by the Hamiltonian  $H_p$ , varies versus time significantly, which coincides with Eq. (10) and Fig. 3(a). In addition, the original pumping Hamiltonian  $H - H'_\omega$  driven populations match the  $H_p$  driven populations well, with tiny



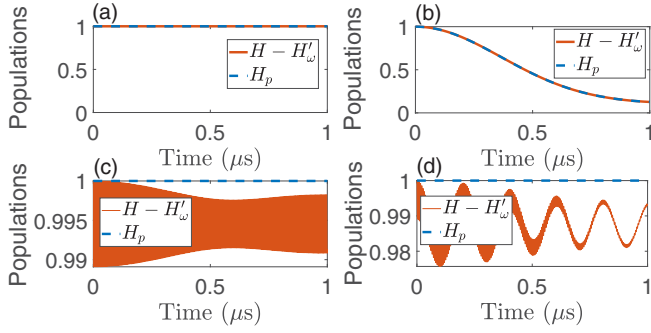


FIG. 4. Populations of (a)  $|00\rangle$ , (b)  $|01\rangle$ , (c)  $|10\rangle$ , and (d)  $|11\rangle$  vs time, under the effective pumping Hamiltonian  $H_p$  driven and original pumping Hamiltonian  $H - H'_\omega$  driven. The relevant parameters read,  $\Omega_2 = 2\pi \times 290.35$  kHz,  $\Omega_e = 1.5\Omega_2 = 2\pi \times 435.53$  kHz,  $\Omega_1 = 24\Omega_2 = 2\pi \times 6.97$  MHz, and  $V_{\text{dip}} = \Delta = 27\Omega_1 = 2\pi \times 188.15$  MHz.

differences in Figs. 4(c) and 4(d) induced by incomplete satisfaction of condition  $V_{\text{dip}} \gg \Omega_1 \gg \{\Omega_2, \Omega_e\}$ .

Up to now, one can know that any state that only contains these three basis  $|00\rangle$ ,  $|10\rangle$ , and  $|11\rangle$  may be the steady state of the system driven by  $H_p$ . The KLM state,  $[|KLM\rangle = (|00\rangle + |10\rangle + |11\rangle)/\sqrt{3}]$ , is the steady state, but not the unique one, which means different initial states will be driven to different final steady states by  $H_p$ . Hence we introduce the “shuffling Hamiltonian”  $H'_\omega$ , to ensure the KLM state is the unique steady state. In the ground state basis  $\{|00\rangle, |01\rangle, |10\rangle, |11\rangle\}$ ,  $H'_\omega$  yields

$$H'_\omega = \begin{pmatrix} 2\Omega_\omega & \Omega_\omega & -\Omega_\omega & 0 \\ \Omega_\omega & \Omega_\omega & 0 & -\Omega_\omega \\ -\Omega_\omega & 0 & \Omega_\omega & \Omega_\omega \\ 0 & -\Omega_\omega & \Omega_\omega & 0 \end{pmatrix}, \quad (11)$$

by setting  $\delta = \Omega_\omega$ . The master equation of  $H'_\omega$  driven system reads

$$\dot{\rho}(t) = -i[H'_\omega, \rho(t)]. \quad (12)$$

Note that the master equation in Eq. (12) does not include decoherence part because there are no exited state during the evolution driven by  $H'_\omega$ . The steady state  $\rho(t_f)$  under  $H'_\omega$  driven should satisfy  $\rho^{(r)}(t_f) = 0$  with  $r$  and  $t_f$  being the derivation order (any positive integer) and the final time, respectively, which holds when  $\dot{\rho}(t_f) = -i[H'_\omega, \rho(t_f)] \equiv 0$ . Thereupon, the eigenstates of  $H'_\omega$ ,

$$\begin{aligned} |\phi_1\rangle &= \frac{5 - \sqrt{5}}{20}[-(3 + \sqrt{5})|00\rangle - (1 + \sqrt{5})|01\rangle \\ &\quad + (1 + \sqrt{5})|10\rangle + 2|11\rangle], \\ |\phi_2\rangle &= \frac{5 + \sqrt{5}}{20}[-(3 - \sqrt{5})|00\rangle - (1 - \sqrt{5})|01\rangle \\ &\quad + (1 - \sqrt{5})|10\rangle + 2|11\rangle], \\ |\phi_3\rangle &= \frac{1}{\sqrt{3}}(|00\rangle + |10\rangle + |11\rangle) = |\text{KLM}\rangle, \\ |\phi_4\rangle &= \frac{1}{\sqrt{15}}(|00\rangle - 3|01\rangle - 2|10\rangle + |11\rangle), \end{aligned} \quad (13)$$

are all the steady states of the system driven by  $H'_\omega$ , but only  $|\phi_3\rangle$ , i.e., the KLM state, just includes bases  $|00\rangle$ ,  $|10\rangle$ , and  $|11\rangle$  and that be the steady state of the system driven by  $H_p$  as well. Thereupon, the KLM state is the unique steady state of the system driven by the effective Hamiltonian,  $H_{\text{eff}} = H_p + H'_\omega$ .

## IV. NUMERICAL SIMULATION

### A. Ideal situation

The original Hamiltonian and effective Hamiltonian are respectively submitted to the master equation

$$\dot{\rho}(t) = i[\rho(t), \bullet] + \sum_{l=1}^{16} L_l \rho(t) L_l^\dagger - \frac{1}{2} [L_l^\dagger L_l \rho(t) + \rho(t) L_l^\dagger L_l], \quad (14)$$

where the big dot,  $\bullet$ , represents different Hamiltonians and  $L_l$  ( $l = 1, 2, \dots, 16$ ) indicate Lindblad operators yielding ( $t = 0, 1$  and  $j = 1, 2$ )

$$\begin{aligned} L_{t+1+8(j-1)} &= \sqrt{\Gamma_e/2}|t\rangle_j \langle e|, & L_{t+3+8(j-1)} &= \sqrt{\Gamma_r/2}|t\rangle_j \langle r|, \\ L_{t+5+8(j-1)} &= \sqrt{\Gamma_p/2}|t\rangle_j \langle p|, & L_{t+7+8(j-1)} &= \sqrt{\Gamma_f/2}|t\rangle_j \langle f|, \end{aligned} \quad (15)$$

which describe the spontaneous emissions from  $|e\rangle$ ,  $|r\rangle$ ,  $|p\rangle$ , and  $|f\rangle$  to  $|0\rangle$  and  $|1\rangle$ . In addition, initial state here is a mixed state  $\rho(0) = (|00\rangle\langle 00| + |01\rangle\langle 01| + |10\rangle\langle 10| + |11\rangle\langle 11|)/4$ . Notice that  $\rho(0)$  is not the only initial state to implement the present protocol. Indeed, arbitrary initial states made up by ground states components can be driven to the KLM states here. The relevant parameters are

$$\begin{aligned} \Gamma_e &= 2\pi \times 1.31 \text{ MHz}, & \Gamma_r &= 2\pi \times 5.0 \text{ kHz}, \\ \Gamma_p &= 2\pi \times 2.1 \text{ kHz}, & \Gamma_f &= 2\pi \times 5.6 \text{ kHz}, \\ \Omega_\omega &= 2\pi \times 145.18 \text{ kHz}, \\ \Omega_2 &= 2\Omega_\omega = 2\pi \times 290.35 \text{ kHz}, \\ \Omega_e &= 1.5\Omega_2 = 2\pi \times 435.53 \text{ kHz}, \\ \Omega_1 &= 24\Omega_2 = 2\pi \times 6.97 \text{ MHz}, \\ V_{\text{dip}} &= \Delta = 27\Omega_1 = 2\pi \times 188.15 \text{ MHz}, \end{aligned} \quad (16)$$

where the value of  $\Omega_1$  is reliable in the experiment [45] and the value of  $V_{\text{dip}}$  corresponds to the atomic distance  $R = 2.673 \mu\text{m}$ . Also, the values of  $\Gamma_e$ ,  $\Gamma_r$ ,  $\Gamma_p$ , and  $\Gamma_f$  approximately correspond to the lifetimes of specific Rb atom states [47,55]. Based on the parameters, we plot the fidelities for the present scheme versus time via full Hamiltonian and effective Hamiltonian in Fig. 5(a). It is visualized in Fig. 5(a) that the full Hamiltonian drives the system to the final state as exactly the effective Hamiltonian does. The fidelity for the fast and dephasing-tolerant preparation of steady KLM states reaches 99.24% at 80  $\mu\text{s}$ , shorter than 1.36 ms in the previous Rydberg-atom-based KLM preparation scheme of Ref. [35]. Meanwhile, when the initial states are not mixed states but pure states, the fidelities driven by the original Hamiltonian are shown in Fig. 5(b), in which one can find the fidelities all reach above 99% in 80  $\mu\text{s}$ .

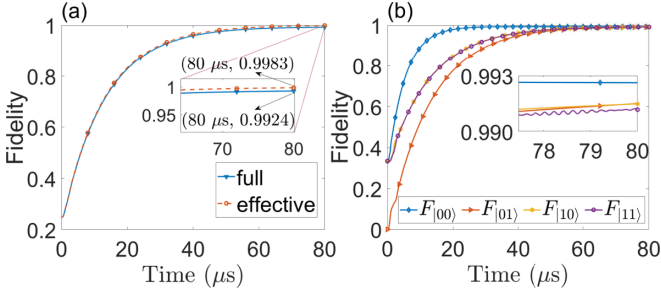


FIG. 5. (a) Fidelities vs time with blue solid line (marking with triangles) and orange dash line (marking with circles) corresponding to full Hamiltonian driven and effective Hamiltonian driven systems, respectively. (b) Fidelities driven by the original Hamiltonian vs. time when the initial states are pure states  $|00\rangle$ ,  $|01\rangle$ ,  $|10\rangle$ , and  $|11\rangle$ . Relevant parameters are shown in Eq. (16).

### B. Atomic dephasing

As mentioned in Sec. I, the optical tweezers in the practical experiment may not exactly fix atoms in specific positions. That is, the real atomic distance may have a little fluctuation, which is  $\delta R/R = 1.89\%$  reported in the experiment [39]. Considering  $V_{\text{dip}} = \sqrt{2}C_3/R^3$ , such a fluctuation in atomic distance may cause  $\delta V_{\text{dip}}/V_{\text{dip}} \simeq 3\delta R/R \sim 6\%$  and further result in the inaccuracy of the effective Hamiltonian.

Specifically, if the Rydberg antiblockade effect is utilized in the present scheme, the effective pumping Hamiltonian reads

$$H'_p = \Omega_{\text{eff}}|01\rangle\langle rr| + \text{H.c.}, \quad (17)$$

with  $\Omega_{\text{eff}} = \frac{2\Omega_1^2}{\Delta}$ , which is utilized in the scheme of Ref. [35] for the preparation of KLM states. When  $\delta V_{\text{dip}}/V_{\text{dip}}$  is small enough, the modified effective Hamiltonian under the atomic dephasing can be given by

$$H''_p = \Omega_{\text{eff}}|01\rangle\langle rr| + \delta V_{\text{dip}}|rr\rangle\langle pf| + \text{H.c.} \quad (18)$$

According to the parameters relation used in Eq. (16),  $\Delta = 27\Omega_1$ ,  $V_{\text{dip}} = \Delta$ , such that,  $\Omega_{\text{eff}} = \frac{2\Delta}{729}$  and  $\delta V_{\text{dip}} = -36\Omega_{\text{eff}} \sim 36\Omega_{\text{eff}}(\delta = -0.1 \sim 0.1)$ , one can find that the dynamical evo-

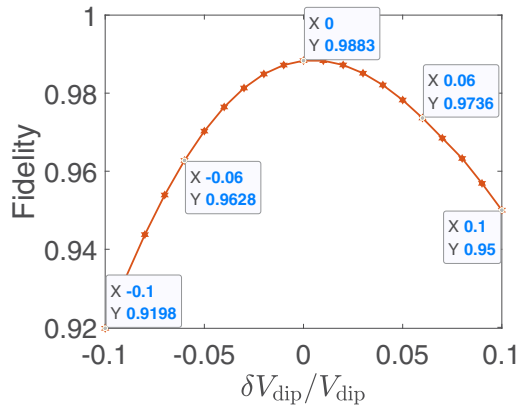


FIG. 6. Fidelity (at 80  $\mu\text{s}$ ) vs  $\delta V_{\text{dip}}/V_{\text{dip}}$ . The initial states for all the points are  $\rho(0) = (|00\rangle\langle 00| + |01\rangle\langle 01| + |10\rangle\langle 10| + |11\rangle\langle 11|)/4$  and the relevant parameters follows Eq. (16) with differences  $\Omega_1 = 40\Omega_2$  and  $\Delta = 15\Omega_1$ .

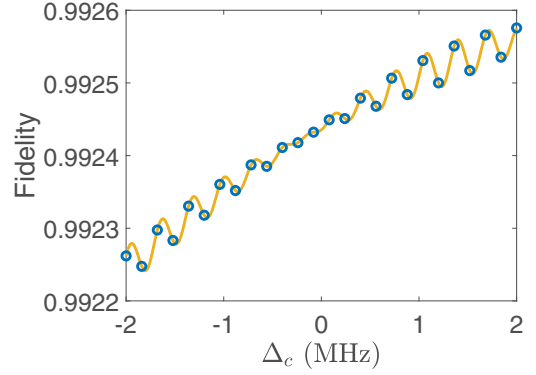


FIG. 7. Fidelity (at 80  $\mu\text{s}$ ) vs  $\Delta_c$ . The initial states for all the points are  $\rho(0) = (|00\rangle\langle 00| + |01\rangle\langle 01| + |10\rangle\langle 10| + |11\rangle\langle 11|)/4$  and the relevant parameters exactly follow Eq. (16). Observe that the influence of  $\Delta_c$  is so tiny that the fidelity exceed 99.24% (when  $\Delta_c = 0$ ) at some points  $\Delta_c \neq 0$ .

lution driven by  $H''_p$  is completely different from that by  $H'_p$ . Therefore the effective pumping Hamiltonian  $H'_p$  is disabled when the atomic dephasing happens.

Hence, when multi-Rydberg states are stimulated during the evolution of system, the atomic dephasing will seriously decrease the efficiencies or fidelities of some Rydberg-atom-based QIP tasks [16,32,35,39,56,57]. A specific comparison is given in Fig. 8 of the scheme of Ref. [58], the fidelities of single-Rydberg-states-populated gates and multi-Rydberg-states-populated gates are respectively 97.06% and 49.65% when  $\delta V_{\text{dip}}/V_{\text{dip}} = 10\%$ .

In fact, for the steady state preparation works, the comparison of fidelity between single-Rydberg-state-populated schemes and multi-Rydberg-state-populated schemes will not be as pronounced. For instance, although the effective pumping Hamiltonian  $H'_p$  in Eq. (17) is disabled, the multi-Rydberg states can dissipate to the ground states to finally keep  $|01\rangle$  unstable, which can be further used to complete the steady KLM states preparation. However, from Eq. (18) and relation  $\delta V_{\text{dip}} = -36\Omega_{\text{eff}} \sim 36\Omega_{\text{eff}}$ , one can find that there is a detuning between  $|01\rangle$  and  $|rr\rangle$ , which will reduce the population of  $|rr\rangle$  during the evolution and thus slow the dissipative speed. In this case, the evolution time will be extended. Ergo, it is

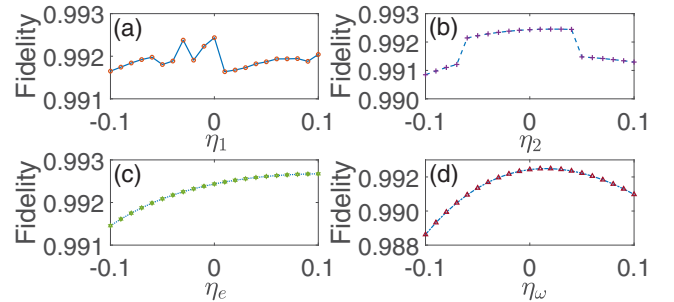


FIG. 8. Fidelities (at 80  $\mu\text{s}$ ) vs (a)  $\eta_1$ , (b)  $\eta_2$ , (c)  $\eta_e$ , and (d)  $\eta_\omega$ . Similarly, the influence of  $\eta_q$  is so slight that at some points  $\eta_q \neq 0$ , the fidelity exceed which at point  $\eta_q = 0$ . The initial states of all the points are still  $\rho(0) = (|00\rangle\langle 00| + |01\rangle\langle 01| + |10\rangle\langle 10| + |11\rangle\langle 11|)/4$  and the relevant parameters follow Eq. (16).

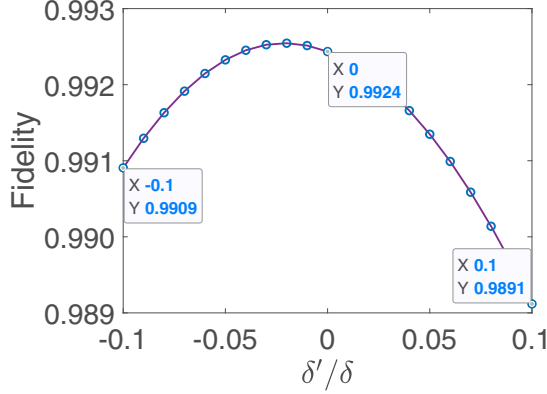


FIG. 9. Fidelity (at  $80 \mu\text{s}$ ) vs  $\delta'/\delta$ . The initial states of all the points are  $\rho(0) = (|00\rangle\langle 00| + |01\rangle\langle 01| + |10\rangle\langle 10| + |11\rangle\langle 11|)/4$  and the relevant parameters follow Eq. (16).

needed to avoid simultaneous excitations of Rydberg atoms in the preparation of steady state.

Here we plot the fidelity for the fast and dephasing-tolerant preparation of steady KLM states versus atomic dephasing rate  $\delta V_{\text{dip}}/V_{\text{dip}}$  in Fig. 6, from which one can see that at point  $\delta V_{\text{dip}}/V_{\text{dip}} = 6\%$  as the experimental observation [39], the fidelity is 97.36%. Even when  $\delta V_{\text{dip}}/V_{\text{dip}} = \pm 10\%$ , the fidelity is still high as 95.00% (91.98%).

### C. Voltage fluctuation

As shown in Fig. 1(a), the experimental model needs an electric fields  $F_{\text{res}} \simeq 32 \text{ mVcm}^{-1}$ , generated by electrodes with a certain voltage, to ensure the Förster resonance. With reference to the experiment [39], the voltage applied to the electrodes will fluctuate a few mVs, inducing fluctuation in  $F_{\text{res}}$  and further in detuning ( $< 1 \text{ MHz}$ ) of  $|rr\rangle$  and  $|pf\rangle$ . For simulating such a phenomenon, the original Hamiltonian shown in Eq. (2) can be modified as

$$H_c = H + \Delta_c |rr\rangle\langle rr|, \quad (19)$$

and further be submitted into Eq. (14). Then we can plot the relation between the fidelity for the fast and dephasing-tolerant preparation of steady KLM states versus  $\Delta_c$  in Fig. 7, where one can see that the fidelity barely decreases when  $\Delta_c$  varies. At point  $\Delta_c = \pm 2 \text{ MHz}$ , the fidelity reaches 99.258% (99.226%), which is acceptable in the experiment.

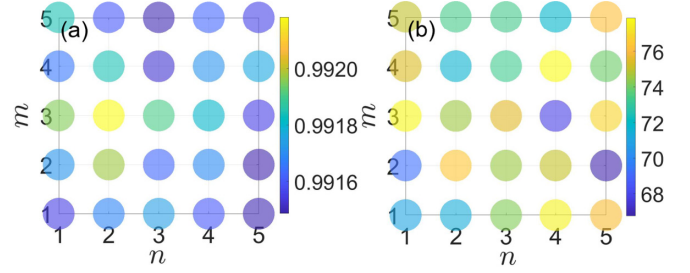


FIG. 10. (a) Fidelity and (b) corresponding evolution time vs  $G_p(p = 5^{m-1} + n)$ . The relevant parameters are the same as that shown in Eq. (16).

### D. Rabi frequencies deviations

In many experimental scenarios, the Rabi frequencies may not be adjusted exactly, generally with several deviations. Such that the real value of Rabi frequency in the experiment should be rewritten as

$$\Omega'_q = (1 + \eta_q)\Omega_q \quad (20)$$

with  $q = 1, 2, e, \omega$  and  $\eta_q$  being the deviation rate of  $\Omega_q$ . For testing whether the present scheme is robust to the deviations of Rabi frequencies or not, we plot the fidelity (driven by the original Hamiltonian) for the fast and dephasing-tolerant preparation of steady KLM states versus  $\eta_q$  in Fig. 8, from which one can find that the fidelity is robust against the deviations of Rabi frequencies. Specifically, all the fidelities remain in 98.8%  $\sim$  99.3% when deviations rates change from  $-10\%$  to  $10\%$ .

It is noteworthy that in Sec. III, we have set the small detuning  $\delta = \Omega_\omega = 2\pi \times 145.18 \text{ kHz}$ , which is generally adjusted with a little deviation about dozens of kHzs, according to the experiment [46] [see Fig. 2(c) of this reference.]. Therefore the fidelity versus the detuning deviation,  $\delta'/2\pi = -14.5 \sim 14.5 \text{ kHz}$ , is plotted in Fig. 9, in which the fidelity is still high as 98.91% (99.01%) when  $\delta'/\delta = \pm 0.1$ . This demonstrates that the present scheme is also robust to the deviation of  $\delta$ .

### E. Arbitrariness of the initial state

In fact, the producing of desired initial states in many schemes are also problems. Such that the arbitrariness of the initial state can be used as an index to test the experimental

TABLE I. Groups of random numbers  $\{\alpha_1, \alpha_2, \alpha_3\}$ .

$G_1 = \{0.5497, 0.6892, 0.2638\}$	$G_2 = \{0.9172, 0.7482, 0.1455\}$	$G_3 = \{0.2858, 0.4505, 0.1361\}$	$G_4 = \{0.7572, 0.0838, 0.8693\}$	$G_5 = \{0.7537, 0.2290, 0.5797\}$
$G_6 = \{0.3804, 0.9133, 0.5499\}$	$G_7 = \{0.5678, 0.1524, 0.1450\}$	$G_8 = \{0.0759, 0.8258, 0.8530\}$	$G_9 = \{0.0540, 0.5383, 0.6221\}$	$G_{10} = \{0.5308, 0.9961, 0.3510\}$
$G_{11} = \{0.7792, 0.0782, 0.5132\}$	$G_{12} = \{0.9340, 0.4427, 0.4018\}$	$G_{13} = \{0.1299, 0.1067, 0.0760\}$	$G_{14} = \{0.5688, 0.9619, 0.2399\}$	$G_{15} = \{0.4694, 0.0046, 0.1233\}$
$G_{16} = \{0.0119, 0.7749, 0.1839\}$	$G_{17} = \{0.3371, 0.8173, 0.2400\}$	$G_{18} = \{0.1622, 0.8687, 0.4173\}$	$G_{19} = \{0.7943, 0.0844, 0.0497\}$	$G_{20} = \{0.3112, 0.3998, 0.9027\}$
$G_{21} = \{0.5285, 0.2599, 0.9448\}$	$G_{22} = \{0.1656, 0.8001, 0.4909\}$	$G_{23} = \{0.6020, 0.4314, 0.4893\}$	$G_{24} = \{0.2630, 0.9106, 0.3377\}$	$G_{25} = \{0.6541, 0.1818, 0.9001\}$

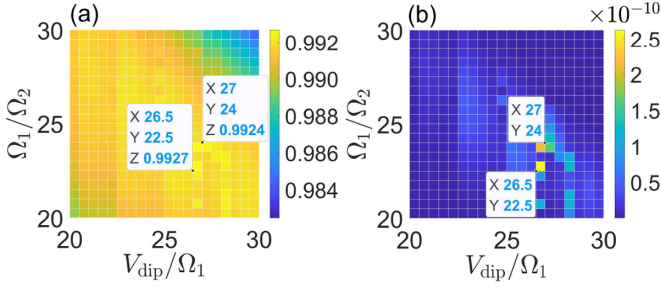


FIG. 11. (a) Fidelity vs  $V_{\text{dip}}/\Omega_1$  and  $\Omega_1/\Omega_2$  at  $80 \mu\text{s}$ . (b) The 3000 power of fidelity vs  $V_{\text{dip}}/\Omega_1$  and  $\Omega_1/\Omega_2$  at  $80 \mu\text{s}$ , which is exhibited here for visually finding the points with higher fidelities.

feasibility of a scheme. From the analysis in Sec. III, we can find that any initial states made up by ground states elements can be driven to the KLM states. For proving it, the initial state is parameterized as

$$\begin{aligned}
 |\psi(0)\rangle = & \cos \alpha_1 |00\rangle + \sin \alpha_1 \cos \alpha_2 |01\rangle \\
 & + \sin \alpha_1 \sin \alpha_2 \cos \alpha_3 |10\rangle \\
 & + \sin \alpha_1 \sin \alpha_2 \sin \alpha_3 |11\rangle,
 \end{aligned} \quad (21)$$

with  $\alpha_k (k = 1, 2, 3)$  being a random number in the range of  $0 - 1$ . Notice that only ground states elements are considered here, since the other elements are all include excited states and will decay to the ground states elements.

We choose 25 groups random numbers of  $\{\alpha_1, \alpha_2, \alpha_3\}$ , represented by  $G_p (p = 1, 2, \dots, 25)$  and shown in Table I. These 25 random initial states are submitted into Eq. (14) with original Hamiltonian shown in Eq. (2). Subsequently we plot the fidelity and corresponding evolution time for the fast and dephasing-tolerant preparation of steady KLM states versus  $G_p (p = 5^{m-1} + n)$  in Figs. 10(a) and 10(b), respectively. It is clear in Fig. 10 that the fidelities for various random initial states are all higher than 99.14% with evolution times about 66–78  $\mu\text{s}$ .

#### F. The tradeoff between fidelity and time

Firstly, we choose parameters conditions

$$\begin{aligned}
 \Omega_2 &= 2\Omega_\omega, \quad \Omega_e = 1.5\Omega_2, \quad \Gamma_e = 9\Omega_\omega, \\
 V_{\text{dip}} &= 2\pi \times 188.15 \text{ MHz}, \quad \Gamma_r = 2\pi \times 5.0 \text{ kHz}, \\
 \Gamma_p &= 2\pi \times 2.1 \text{ kHz}, \quad \Gamma_f = 2\pi \times 5.6 \text{ kHz},
 \end{aligned} \quad (22)$$

to plot the fidelity versus  $V_{\text{dip}}/\Omega_1$  and  $\Omega_1/\Omega_2$  at  $80 \mu\text{s}$  in Fig. 11 and find two points with relatively high fidelities:  $\{V_{\text{dip}}/\Omega_1 = 27, \Omega_1/\Omega_2 = 24, 99.24\% \}$  and  $\{V_{\text{dip}}/\Omega_1 = 26.5, \Omega_1/\Omega_2 = 22.5, 99.27\% \}$ . We consider these two points as the optimal points and the former one is used in Eq. (16).

Furthermore, we can search the other optimal points with different evolution time by plotting corresponding contour maps like Fig. 11. For the simplicity, the other contour maps of the fidelities with different evolution time are not placed here. While the final optimal results are shown in Table II, from which one can find that the fidelity slowly increase as the evolution time substantially extending. For instance, the fidelity can reach 99.9% with the evolution time increasing to

TABLE II. Optimal fidelities with corresponding time.

$V_{\text{dip}}/\Omega_1$	$\Omega_1/\Omega_2$	Time	Fidelity
11	9.5	10 $\mu\text{s}$	96.30%
16.5	11	20 $\mu\text{s}$	98.05%
24.5	13	40 $\mu\text{s}$	98.94%
27	24	80 $\mu\text{s}$	99.24%
26.5	22.5	80 $\mu\text{s}$	99.27%
28	33	160 $\mu\text{s}$	99.62%
48	49	400 $\mu\text{s}$	99.78%
59	64	800 $\mu\text{s}$	99.85%
82	81	1200 $\mu\text{s}$	99.90%

1200  $\mu\text{s}$ . On the other hand, the fidelity is very close to 99% when the evolution time is 40  $\mu\text{s}$ .

#### V. CONCLUSION

We proposed a scheme for fast and dephasing-tolerant preparation of steady KLM states. The Förster resonance effect was utilized here to build strong dipole-dipole interaction ( $2\pi \times 188.15 \text{ MHz}$ ), leading to a shorter evolution time (80  $\mu\text{s}$ ). In addition, we avoided simultaneously stimulating multiple Rydberg states during the whole preparation process. Such that the influence of the atomic dephasing noise is slight in the present scheme.

Specifically, the present scheme has several advantages as follows.

(i) Fast. Compared with evolution time of the representative work [35] of Rydberg-atom-based steady KLM preparation, 1.36 ms, the present scheme is faster (80  $\mu\text{s}$ , see Fig. 12) and perhaps seems more suitable for some rapid quantum information tasks based on the Rydberg atoms [59–74].

(ii) Tolerance to the atomic dephasing. As is known that the atomic dephasing always plays a role of a stumbling block in various Rydberg-atom-based processes [16,32,35,39,56,57].

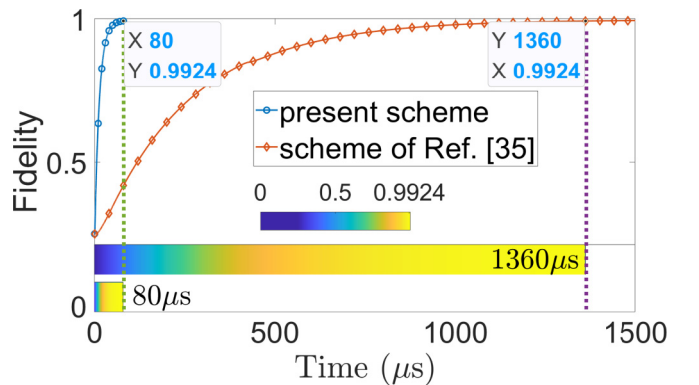


FIG. 12. Comparative diagram of operation time between the present scheme and the scheme of Ref. [35]. Note that we choose the same dipole-dipole interaction energy,  $V_{\text{dip}} = 2\pi \times 188.15 \text{ MHz}$ , to plot this comparative diagram and the parameters relations we used here to plot the fidelity curve of the scheme of Ref. [35] is the same as that in Fig. 5 in Ref. [35], i.e.,  $V_{\text{dip}} = 90\Omega = 18000\gamma$ . The initial states are all  $\rho(0) = (|00\rangle\langle 00| + |01\rangle\langle 01| + |10\rangle\langle 10| + |11\rangle\langle 11|)/4$ .



In the present scheme, we successfully suppressed the influence caused by the atomic dephasing. When considering the dephasing rate  $\delta V_{\text{dip}}/V_{\text{dip}} = 6\%$  follows the real experimental scenario [39], the fidelity is still high as 97.36%.

(iii) Robust to the deviations of Rabi frequencies. The fidelity maintain as 98.8%–99.3% when the deviation rates vary from  $-10\%$  to  $10\%$ .

(iv) Arbitrariness of the initial state. The initial state of the present scheme can be any states, which all lead fidelities higher than 99.14%.

Thereby, the present scheme is suitable for experimentally producing the KLM states and may enrich the research of dissipative preparation in the Rydberg-atom-based system.

Sincerely, we hope the scheme can be considered applying in the upcoming experiments.

#### ACKNOWLEDGMENTS

This work was supported by the National Natural Science Foundation of China under Grants No. 11575045, No. 11874114, No. 11674060, No. 11805036, No. 11804308, and the Natural Science Funds for Distinguished Young Scholar of Fujian Province under Grant 2020J06011, Project from Fuzhou University under Grant JG202001-2, and Natural Science Foundation of Henan Province (202300410481). Y.-H. Chen is supported by the Japan Society for the Promotion of Science (JSPS) KAKENHI Grant No. JP19F19028.

- 
- [1] C. H. Bennett, G. Brassard, C. Crépeau, R. Jozsa, A. Peres, and W. K. Wootters, *Phys. Rev. Lett.* **70**, 1895 (1993).
- [2] D. Bouwmeester, J.-W. Pan, K. Mattle, M. Eibl, H. Weinfurter, and A. Zeilinger, *Nature (London)* **390**, 575 (1997).
- [3] M. Riebe, H. Häffner, C. F. Roos, W. Hänsel, J. Benhelm, G. P. T. Lancaster, T. W. Körber, C. Becher, F. Schmidt-Kaler, D. F. V. James, and R. Blatt, *Nature (London)* **429**, 734 (2004).
- [4] A. K. Ekert, *Phys. Rev. Lett.* **67**, 661 (1991).
- [5] C. H. Bennett, F. Bessette, G. Brassard, L. Salvail, and J. Smolin, *J. Cryptology* **5**, 3 (1992).
- [6] N. Gisin, G. Ribordy, W. Tittel, and H. Zbinden, *Rev. Mod. Phys.* **74**, 145 (2002).
- [7] A. M. Lance, T. Symul, W. P. Bowen, B. C. Sanders, and P. K. Lam, *Phys. Rev. Lett.* **92**, 177903 (2004).
- [8] F.-G. Deng, X.-H. Li, C.-Y. Li, P. Zhou, and H.-Y. Zhou, *Phys. Rev. A* **72**, 044301 (2005).
- [9] M. B. Plenio, S. F. Huelga, A. Beige, and P. L. Knight, *Phys. Rev. A* **59**, 2468 (1999).
- [10] A. Beige, *Phys. Rev. A* **69**, 012303 (2004).
- [11] B. Kraus, H. P. Büchler, S. Diehl, A. Kantian, A. Micheli, and P. Zoller, *Phys. Rev. A* **78**, 042307 (2008).
- [12] S. Diehl, A. Micheli, A. Kantian, B. Kraus, H. P. Büchler, and P. Zoller, *Nat. Phys.* **4**, 878 (2008).
- [13] F. Verstraete, M. M. Wolf, and J. I. Cirac, *Nat. Phys.* **5**, 633 (2009).
- [14] X.-T. Wang and S. G. Schirmer, *arXiv:1005.2114*.
- [15] M. J. Kastoryano, F. Reiter, and A. S. Sørensen, *Phys. Rev. Lett.* **106**, 090502 (2011).
- [16] A. W. Carr and M. Saffman, *Phys. Rev. Lett.* **111**, 033607 (2013).
- [17] D. D. Bhaktavatsala Rao and K. Mølmer, *Phys. Rev. Lett.* **111**, 033606 (2013).
- [18] F. Reiter, A. S. Sørensen, P. Zoller, and C. A. Muschik, *Nat. Commun.* **8**, 1822 (2017).
- [19] Y.-H. Chen, Z.-C. Shi, J. Song, Y. Xia, and S.-B. Zheng, *Phys. Rev. A* **97**, 032328 (2018).
- [20] Z. Jin, S.-L. Su, and S. Zhang, *Phys. Rev. A* **100**, 052332 (2019).
- [21] Y. Wang, C.-S. Hu, Z.-C. Shi, B.-H. Huang, J. Song, and Y. Xia, *Ann. Phys. (Berlin)* **531**, 1900006 (2019).
- [22] H. Krauter, C. A. Muschik, K. Jensen, W. Wasilewski, J. M. Petersen, J. I. Cirac, and E. S. Polzik, *Phys. Rev. Lett.* **107**, 080503 (2011).
- [23] J. T. Barreiro, M. Müller, P. Schindler, D. Nigg, T. Monz, M. Chwalla, M. Hennrich, C. F. Roos, P. Zoller, and R. Blatt, *Nature (London)* **470**, 486 (2011).
- [24] Y. Lin, J. P. Gaebler, F. Reiter, T. R. Tan, R. Bowler, A. S. Sørensen, D. Leibfried, and D. J. Wineland, *Nature (London)* **504**, 415 (2013).
- [25] S. Shankar, M. Hatridge, Z. Leghtas, K. M. Sliwa, A. Narla, U. Vool, S. M. Girvin, L. Frunzio, M. Mirrahimi, and M. H. Devoret, *Nature (London)* **504**, 419 (2013).
- [26] M. Saffman, T. G. Walker, and K. Mølmer, *Rev. Mod. Phys.* **82**, 2313 (2010).
- [27] H. Weimer, M. Müller, I. Lesanovsky, P. Zoller, and H. P. Büchler, *Nat. Phys.* **6**, 382 (2010).
- [28] T. E. Lee, H. Häffner, and M. C. Cross, *Phys. Rev. A* **84**, 031402(R) (2011).
- [29] D. D. Bhaktavatsala Rao and K. Mølmer, *Phys. Rev. A* **90**, 062319 (2014).
- [30] X.-Q. Shao, J.-B. You, T.-Y. Zheng, C. H. Oh, and S. Zhang, *Phys. Rev. A* **89**, 052313 (2014).
- [31] S.-L. Su, Q. Guo, H.-F. Wang, and S. Zhang, *Phys. Rev. A* **92**, 022328 (2015).
- [32] X. Q. Shao, J. H. Wu, X. X. Yi, and G.-L. Long, *Phys. Rev. A* **96**, 062315 (2017).
- [33] D. X. Li and X. Q. Shao, *Phys. Rev. A* **98**, 062338 (2018).
- [34] Y.-H. Chen, W. Qin, and F. Nori, *Phys. Rev. A* **100**, 012339 (2019).
- [35] D.-X. Li, X.-Q. Shao, J.-H. Wu, X. X. Yi, and T.-Y. Zheng, *Opt. Express* **26**, 2292 (2018).
- [36] S.-L. Su, *arXiv:2006.06529*.
- [37] X.-Q. Shao, *Phys. Rev. A* **102**, 053118 (2020).
- [38] M. Fleischhauer, A. Imamoglu, and J. P. Marangos, *Rev. Mod. Phys.* **77**, 633 (2005).
- [39] S. Ravets, H. Labuhn, D. Barredo, L. Béguin, T. Lahaye, and A. Browaeys, *Nat. Phys.* **10**, 914 (2014).
- [40] E. Knill, R. Laflamme, and G. J. Milburn, *Nature (London)* **409**, 46 (2001).
- [41] T. G. Walker and M. Saffman, *J. Phys. B* **38**, S309 (2005).
- [42] T. G. Walker and M. Saffman, *Phys. Rev. A* **77**, 032723 (2008).
- [43] L. Béguin, A. Vernier, R. Chicireanu, T. Lahaye, and A. Browaeys, *Phys. Rev. Lett.* **110**, 263201 (2013).
- [44] A. Reinhard, T. C. Liebisch, B. Knuffman, and G. Raitel, *Phys. Rev. A* **75**, 032712 (2007).

- [45] T. Wilk, A. Gaëtan, C. Evellin, J. Wolters, Y. Miroshnychenko, P. Grangier, and A. Browaeys, *Phys. Rev. Lett.* **104**, 010502 (2010).
- [46] Y.-Y. Jau, A. M. Hankin, T. Keating, I. H. Deutsch, and G. W. Biedermann, *Nat. Phys.* **12**, 71 (2015).
- [47] C. E. Theodosiou, *Phys. Rev. A* **30**, 2881 (1984).
- [48] D. F. James and J. Jerke, *Can. J. Phys.* **85**, 625 (2007).
- [49] C. Ates, T. Pohl, T. Pattard, and J. M. Rost, *Phys. Rev. Lett.* **98**, 023002 (2007).
- [50] T. Amthor, C. Giese, C. S. Hofmann, and M. Weidemüller, *Phys. Rev. Lett.* **104**, 013001 (2010).
- [51] Z. Zuo and K. Nakagawa, *Phys. Rev. A* **82**, 062328 (2010).
- [52] T. E. Lee, H. Häffner, and M. C. Cross, *Phys. Rev. Lett.* **108**, 023602 (2012).
- [53] W. Li, C. Ates, and I. Lesanovsky, *Phys. Rev. Lett.* **110**, 213005 (2013).
- [54] S.-L. Su, E. Liang, S. Zhang, J.-J. Wen, L.-L. Sun, Z. Jin, and A.-D. Zhu, *Phys. Rev. A* **93**, 012306 (2016).
- [55] I. I. Beterov, I. I. Ryabtsev, D. B. Tretyakov, and V. M. Entin, *Phys. Rev. A* **79**, 052504 (2009).
- [56] S.-L. Su, F.-Q. Guo, L. Tian, X.-Y. Zhu, L.-L. Yan, E.-J. Liang, and M. Feng, *Phys. Rev. A* **101**, 012347 (2020).
- [57] R.-H. Zheng, Y.-H. Kang, D. Ran, Z.-C. Shi, and Y. Xia, *Phys. Rev. A* **101**, 012345 (2020).
- [58] R.-H. Zheng, Y.-H. Kang, S.-L. Su, J. Song, and Y. Xia, *Phys. Rev. A* **102**, 012609 (2020).
- [59] C. Gaul, B. J. DeSalvo, J. A. Aman, F. B. Dunning, T. C. Killian, and T. Pohl, *Phys. Rev. Lett.* **116**, 243001 (2016).
- [60] H. Labuhn, D. Barredo, S. Ravets, S. de Léséleuc, T. Macrì, T. Lahaye, and A. Browaeys, *Nature (London)* **534**, 667 (2016).
- [61] J. Zeiher, R. van Bijnen, P. Schauß, S. Hild, J. yoon Choi, T. Pohl, I. Bloch, and C. Gross, *Nat. Phys.* **12**, 1095 (2016).
- [62] L. Li and A. Kuzmich, *Nat. Commun.* **7**, 13618 (2016).
- [63] G. Higgins, F. Pokorny, C. Zhang, Q. Bodart, and M. Hennrich, *Phys. Rev. Lett.* **119**, 220501 (2017).
- [64] H. Bernien, S. Schwartz, A. Keesling, H. Levine, A. Omran, H. Pichler, S. Choi, A. S. Zibrov, M. Endres, M. Greiner, V. Vuletić, and M. D. Lukin, *Nature (London)* **551**, 579 (2017).
- [65] E. Distante, P. Farrera, A. Padrón-Brito, D. Paredes-Barato, G. Heinze, and H. de Riedmatten, *Nat. Commun.* **8**, 14072 (2017).
- [66] F. Engel, T. Dieterle, T. Schmid, C. Tomschitz, C. Veit, N. Zuber, R. Löw, T. Pfau, and F. Meinert, *Phys. Rev. Lett.* **121**, 193401 (2018).
- [67] J. P. Shaffer, S. T. Rittenhouse, and H. R. Sadeghpour, *Nat. Commun.* **9**, 1965 (2018).
- [68] C. G. Wade, M. Marcuzzi, E. Levi, J. M. Kondo, I. Lesanovsky, C. S. Adams, and K. J. Weatherill, *Nat. Commun.* **9**, 3567 (2018).
- [69] A. Deller and S. D. Hogan, *Phys. Rev. Lett.* **122**, 053203 (2019).
- [70] J. P. Covey, I. S. Madjarov, A. Cooper, and M. Endres, *Phys. Rev. Lett.* **122**, 173201 (2019).
- [71] F. Yang, S. Yang, and L. You, *Phys. Rev. Lett.* **123**, 063001 (2019).
- [72] M. Mizoguchi, Y. Zhang, M. Kunimi, A. Tanaka, S. Takeda, N. Takei, V. Bharti, K. Koyasu, T. Kishimoto, D. Jaksch, A. Glaetzle, M. Kiffner, G. Masella, G. Pupillo, M. Weidemüller, and K. Ohmori, *Phys. Rev. Lett.* **124**, 253201 (2020).
- [73] A. Deller, M. H. Rayment, and S. D. Hogan, *Phys. Rev. Lett.* **125**, 073201 (2020).
- [74] M. Stecker, R. Nold, L.-M. Steinert, J. Grimm, D. Petrosyan, J. Fortágh, and A. Günther, *Phys. Rev. Lett.* **125**, 103602 (2020).